Direct comparison of RADARSAT Constellation Mission InSAR, UAV derived point cloud comparison & RTK GNSS deformation monitoring at North Slide, Thompson River Valley, British Columbia

Drew Rotheram-Clarke, Dr. David Huntley, Philip LeSueur, Robert Cocking & Jamel Joseph
Geological Survey of Canada, Pacific Division, Vancouver, British Columbia, Canada
Roger MacLeod,
Geological Survey of Canada, Pacific Division, Victoria, British Columbia, Canada

ABSTRACT
In this research we present results and comparisons of several generally accepted land deformation measurement techniques for monitoring slow moving landslides. We demonstrate these methods along a high-risk section of the national railway transportation corridor traversing the Thompson River valley in the British Columbia interior. These results focus on the geomorphically active North Slide, which acts as an ideal field laboratory for testing and evaluating novel monitoring techniques and methods.

Differential processing of Structure from Motion (SfM) products such as point cloud elevation models and orthophotos derived from Remotely Piloted Aircraft Systems (RPAS) are compared with satellite-based Interferometric Synthetic Aperture RADAR (InSAR) deformation measurements derived from RADARSAT Constellation Mission (RCM). These results are ground-truthed with periodic real-time kinematic (RTK) global navigation satellite system (GNSS) measurements.

Several point cloud comparison techniques, including the popular multi-scale model to model cloud comparison (M3C2) algorithm as well as digital ortho-image correlation techniques are presented. Multitemporal InSAR deformation measurements are processed using a semi-automated processing system for interferogram generation and unwrapping. Small baseline subset (SBAS) processing is done manually to recover 1-dimensional line-of-sight deformation measurements.

Finally, we discuss the strengths and limitations of these techniques, considerations for interpreting their outputs as well as specific considerations for direct comparisons between InSAR, SfM and RTK deformation measurements.

RÉSUMÉ
Dans cette recherche, nous présentons les résultats et les comparaisons de plusieurs techniques de mesure de la déformation du sol généralement acceptées pour la surveillance des glissements de terrain à déplacement lent. Nous démontrons ces méthodes le long d'une section à haut risque du couloir de transport ferroviaire national traversant la vallée de la rivière Thompson dans l'intérieur de la Colombie-Britannique. Ces résultats se concentrent sur le glissement nord, actif sur le plan géomorphologique, qui constitue un laboratoire de terrain idéal pour tester et évaluer de nouvelles techniques et méthodes de surveillance.

Le traitement différentiel des produits de Structure from Motion (SFM), tels que les modèles d'élévation de nuages de points et les orthophotos dérivés des systèmes d'aéronefs téléguidés (RPAS), est comparé aux mesures de déformation par RADAR interférométrique à synthèse d'ouverture (InSAR) dérivées de la mission de la Constellation RADARSAT (RCM). Ces résultats sont vérifiés au sol à l'aide de mesures périodiques de la cinématique en temps réel (RTK) du système mondial de navigation par satellite (GNSS).

Plusieurs techniques de comparaison de nuages de points, dont l'algorithme populaire de comparaison de nuages de modèles à modèles (M3C2), ainsi que des techniques de corrélation d'ortho-images numériques sont présentées. Les mesures de déformation multitemporelles RCM InSAR sont traitées à l'aide d'un système de traitement semi-automatique pour la génération et le déballage des interférogrammes. Le traitement des sous-ensembles de petites lignes de base (SBAS) est effectué manuellement pour récupérer les mesures de déformation à une dimension en ligne de visée et à deux dimensions.

Enfin, nous discutons des forces et des limites de ces techniques, des considérations pour interpréter leurs résultats ainsi que des considérations spécifiques pour les comparaisons directes entre les mesures de déformation InSAR, RPAS et RTK.

1 INTRODUCTION

Landslides pose a risk to the Canadian National (CN) and Canadian Pacific (CP) railways within the Thompson River valley between Ashcroft and Spences Bridge in southern British Columbia (Figure 1) (Clague et al. 2003; Eshraghian et al. 2007). Monitoring these landslides is a priority for Natural Resources Canada (NRCan), the Geological Survey of Canada (GSC), CN, CP and Transport Canada (TC) because of the safety risk, the economic importance, and the need to understand and characterize landslide movement in response to various environmental factors.

The remoteness of these corridors requires monitoring systems that are flexible in their deployment, capable of measuring wide areas, require little or no maintenance and are capable of providing frequent measurements. The Covid-19 pandemic has also particularly highlighted the value of monitoring systems that can continue to provide information without the need for physical site access.

This research builds on previous research efforts in this corridor (Huntley et al. 2017; Journault et al. 2018; Huntley et al. 2021). We present a direct comparison of ground-based (RTK), airborne (SfM) and space-based (InSAR) landslide deformation measurements of the North Slide (Figure 2) as a test case and discuss the strength, limitations and interpretation considerations of each approach.

2 NORTH SLIDE - LANDSLIDE CHARACTERISTICS

The North Slide (Figures 1 & 2) is a retrogressive flow slide that released from the Thompson River eastern valley slope on October 14, 1880 (Stanton 1898; Evans 1984; Clague et al. 2003). In 2000, the toe of this slope reactivated and has since been moving at creep rates. The initial failure occurred after the summer months at a time when terraces were intensively irrigated for agricultural land use, and the toe slope was incised and over-steepened during railway construction.

The slide's main body, including the toe slope, comprises glaciolacustrine sandy silt and sandy gravel outwash unconformably overlying silty till and glaciolacustrine silt and clay (Porter et al. 2002; Clague et al. 2003; Eshraghian et al. 2007; 2008). Porter et al. (2002) reported that a prominent toe bulge and rhythmically interbedded layers of soft brown clay, stiff, high plastic dark grey clay, and grey silt were exposed on the river floodplain (Figure 3). Inclinometer monitoring revealed preferential shearing in soft brown clay beds, with rupture zones at 264 and 269 m above sea level (asl), equivalent to 25 and 30 m below the CP rail grade, and 5 to 10 m below the 2002 river bed. Piezometer data indicated hydrostatic conditions at depth below the track, and an upward gradient in the landslide toe (Porter et al. 2002).

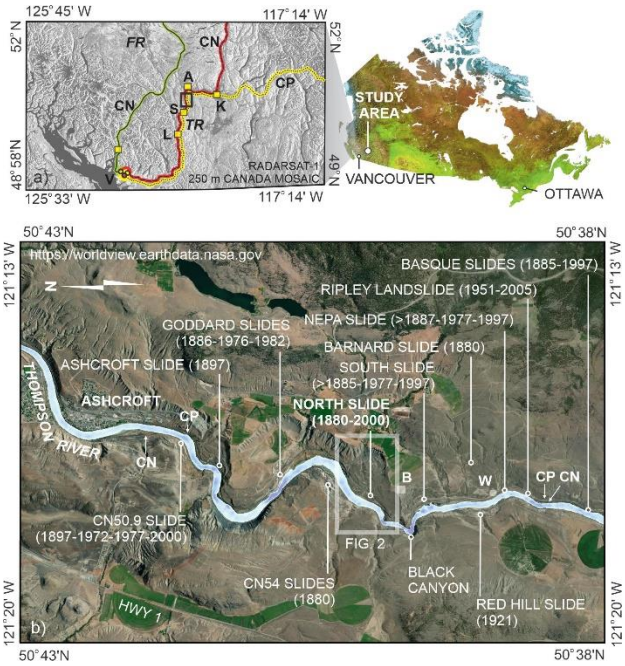

Figure 1. Location of the study area (black rectangle). (a) Rail transportation corridors in southwestern British Columbia with the location of the Thompson River valley: CN: Canadian National Railways; CP: Canadian Pacific Railways A: Ashcroft; K: Kamloops; L: Lytton; S: Spences Bridge; V: Vancouver; FR: Fraser River; TR - Thompson River. (b) Landslide history of the Thompson River valley, showing the location of Ashcroft and the railway transportation corridor in relation to the North Slide survey site; prime ground control point, survey base station (B); and weather station (W).

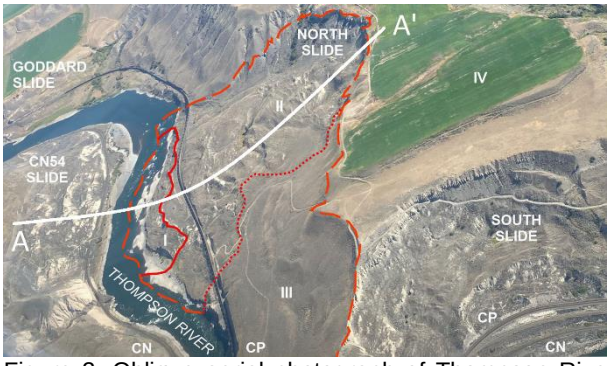

Figure 2. Oblique aerial photograph of Thompson River, the Goddard, North and South slides affecting the CP track, and CN track crossing the CN54 Slide, view to the northeast (I) an active slide toe (0.08 km^2), also known as the solar slump; (II) inactive slide main body and headscarp (0.55 km^2); (III) inactive slide body (0.37 km^2); (IV) stable postglacial slopes and terraces. CN: Canadian National Railways; CP: Canadian Pacific Railways; TR: Thompson River. (August 2020) (NRCAN photo # 2021-035).

In October 2000, movement along 150 m of the toe of the North Slide (the “Solar Slump”) (Figure 3) resulted in between 5 and 15 cm of vertical displacement at the CP grade. Slope inclinometer monitoring between October 2000 and May 2002 measured peak movement rates of approximately 15 cm/year with an average rate of 3 cm/year (Porter et al. 2002). From 5 to 11 cm/year of movement was measured on a shallow rupture surface; while on the deeper slide surface, a movement rate of 3 to 4.5 cm/year was recorded with borehole inclinometers (Porter et al. 2002).

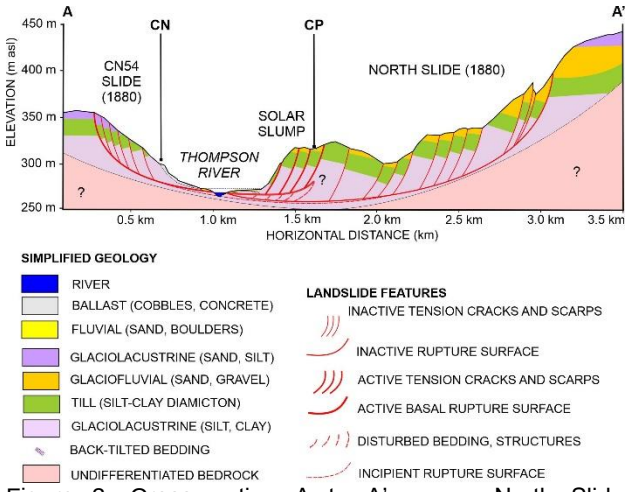

Figure 3. Cross-section A to A’ across North Slide modeled as a rotational-translational landslide in glacial deposits confined to a bedrock paleochannel or basin (after Clague and Evans 2003; Eshraghian et al. 2007; Eshraghian et al. 2008; Porter et al. 2002). See Figure 2 for the location of this cross-section.

Mercury switch tip-over posts linked to rail signals were subsequently installed to monitor for ground displacement and reduce the risk of a train derailment. Since 2001, movements at the rail grade have been managed through regular maintenance and track lifting operations. The slide toe remained active between 2013 and 2015. Persistent scatterer interferometry of RS2 image stacks from 2013 to 2015 identified displacement of coherent targets indicating line-of-sight deformation rates in excess of 5 cm/year, and these were used to coarsely delineate the area of surface displacement (Huntley et al. 2017; Journault et al. 2018).

3 METHODS

The following section summarizes monitoring data collected at North Slide between 2019 and 2021 including change detection techniques used to identify ground movements.

3.1 RPAS Surveying

Two RPAS surveys were flown using a DJI Phantom 4 (Figure 4). This particular RPAS is equipped with a 12.4 Megapixel FC330 which outputs 3000x4000 pixel images. These images are geotagged by the on board GNSS receiver, however since no real-time or post-processing correction is applied to these coordinate information tags, manual ground control is required. This was achieved using ground-based RTK surveying measurements.

The digital optical imagery collected from these surveys was processed using Pix4D Mapper to produce optical ortho-photos at 2 cm ground sample distance (GSD), an elevation point cloud, and a digital surface model (DSM) with a 5 cm ground sample distance. Two surveys were conducted separated by approximately 2 years, (September 19 2019, and September 28 2021). Nearly matching dates were chosen for comparison to mitigate seasonal effects while allowing movement to accumulate to detectable levels. Two post processing techniques for calculating deformation from these data were evaluated, M3C2 and a combination of digital image correlation and DSM of difference.


Figure 4. DJI Phantom 4 RPAS (NRCan Photo 2020-845)

3.2 M3C2 Point Cloud Comparison

The Multiscale Model to Model Cloud Comparison (M3C2) algorithm was introduced to fill a perceived gap in time-series point cloud comparison (Lague et al. 2013). This algorithm has three key characteristics;

- It operates directly on point clouds without the need to grid or mesh one or both point clouds.
- It calculates displacement along a vector normal to the local surface topography.
- It estimates confidence intervals for the measured displacement of changes in the point cloud positions.

The algorithm functions with two basic steps:

1. It first calculates a surface normal at each point by considering a neighbourhood of surrounding points which can be controlled as a user defined neighbourhood search diameter.

2. It then considers two neighbourhoods surrounding each point, often a subset of the points used to define the surface normal and calculates the average distance between the two

different point clouds along the surface normal vector.

This algorithm is well suited for complex situations such as steep topographic settings where rockfalls or toppling of vertical and sub-vertical rock cannot accurately be modeled by simpler methods such as Digital Elevation Model (DEM) differencing. The fundamental assumption of this algorithm is that deformation occurs on a vector normal to the ground surface. This may be a reasonable assumption for some cases, such as the measurement of sediment erosion and redeposition. However, this assumption leads to underestimating displacement in cases where the ground movement is parallel to the surface (Figure 5) which is common in earthflows and translational slides. M3C3 output distances along with the horizontal projection of the surface normal vectors for deformation at North Slide between 2019-09-19 and 2021-09-28 are depicted in Figure 6.

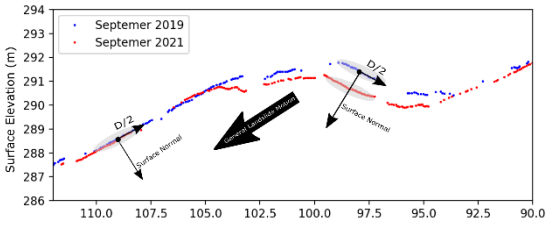

Figure 5. Conceptual diagram of how M3C2 calculates displacement along surface normal vectors. Note the insensitivity to surface parallel flow.

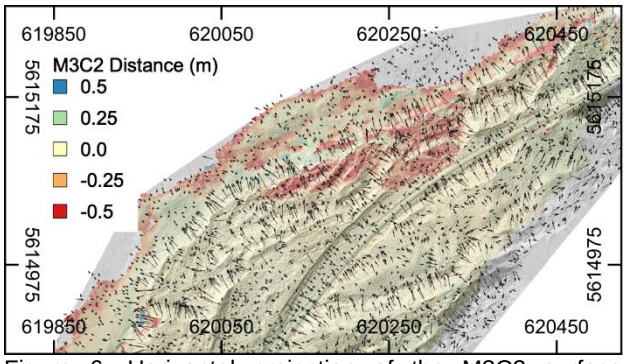

Figure 6. Horizontal projection of the M3C2 surface normals (vectors) over M3C2 distance (raster). Hill-shade transparency is applied for context. All M3C2 surface normal are unit vectors, therefore shorter vectors have a larger vertical component while longer vectors have a larger horizontal component.

3.3 Digital Image Correlation:

Digital Image correlation has been demonstrated as a robust technique for measuring lateral displacement in multi-temporal remote sensing imagery captured from satellites, (Rosu et al. 2015; Türk, 2018) RPAS, (Lucieer et al. 2014) and even handheld cameras in laboratory models (Galland, 2016). Digital image correlation functions within the MicMac software package (Rupnik et al. 2017) were used to calculate subpixel offsets between precisely coregistered imagery. This was tested on both RPAS ortho-photos and hill-shaded Digital Surface Models (DSMs) derived using Structure from Motion methods. However, it was found that the hill-shaded DSMs produced less noisy outputs. We suspect this is a result of the uniformity of the input images which contain fewer differences in dynamic range, changes to vegetation or changes in the surface texture. Combining these results with change detection results derived from DEM differencing (Figure 7) was the only method tested capable of recovering the full 3D deformation vector with wide coverage. We refer to this combined technique subsequently as 3D RPAS.

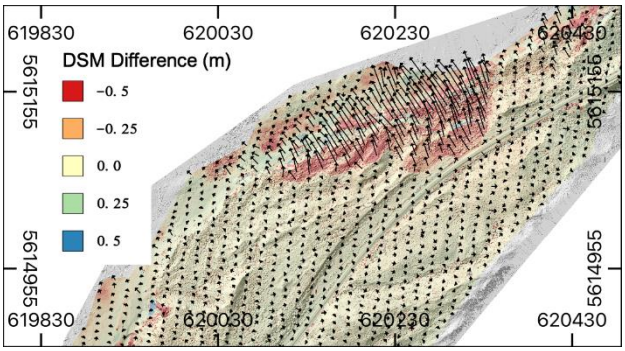

Figure 7. 3D RPAS deformation over North Slide between 2019-09-19 and 2021-09-28. Vectors indicate horizontal deformation from MicMac digital image correlation and colour scale represents the difference in DSMs. Hillshade transparency is applied for context.

3.4 RTK Surveying

Ground control points located within the landslide mass were manually surveyed between September 1st 2019 and March 24th 2022 approximately every 3 - 6 months, in order to monitor ground surface displacements (Figure 8). These measurements were also used to constrain the SfM models, and benchmark deformation derived from RPAS and InSAR measurements.

RTK surveys were completed using a Spectra SP80 GNSS system. First, a stable point outside the landslide mass was selected and surveyed. A long length of rebar, approximately 60 cm in length was driven into stable ground approximately 1 km south of the study site and marked precisely with a 2 mm punch to identify the point. The site was occupied for 12 hours and the GNSS observations were post-processed using Precise Point Positioning software. Subsequent surveys reoccupied this known reference point with a base station. Second, heavy boulders embedded in landslide blocks of interest were marked in with a cross pattern typical of airphoto ground control points (GCPs) using orange survey paint that is highly visible in RPAS imagery. The centres of these patterns were then drilled with a rock drill to ensure exact repeat occupation. These RTK measurements were used to constrain the RPAS SfM measurements, but also provided a means of benchmarking deformation measurements derived from RPAS and InSAR measurements.

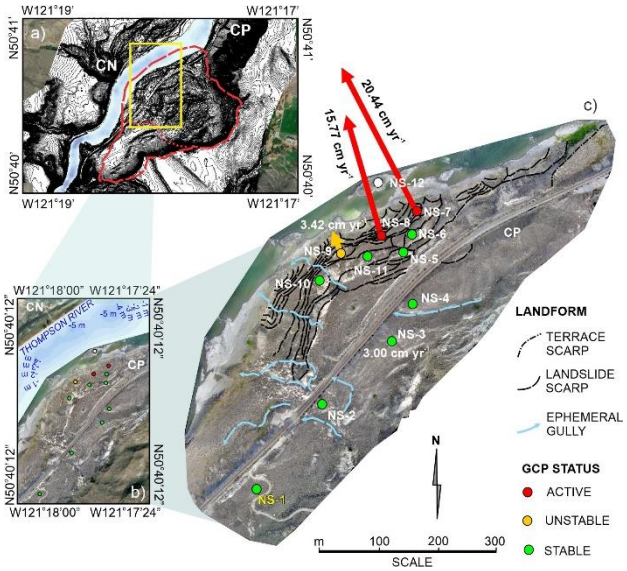

Figure 8. RTK GCP Measurements showing scaled horizontal movement vectors plotted on annotated RPAS digital ortho image; a) DEM derived from 1 m resolution LiDAR; b) bathymetry of Thompson River in the vicinity of the slide; c) location of GCPs (NS-1, NS-2 etc.) and displacement across the toe slope.

3.5 InSAR

A stack of 3-metre resolution RCM descending images were tasked and acquired by the Canadian Space Agency (CSA). The SAR Toolbox in the Earth Observation Data Management System (Dudley et al. 2020) was used to generate interferometric pairs which were then corrected for spatial atmospheric errors, unwrapped and masked for low coherence. This network of unwrapped phase measurements spanning January 5th 2021 to December 3rd 2021 were manually examined and InSAR pairs which contained obvious unwrapping errors or significant phase decorrelation were removed. MsBASv3 which is a freely available SBAS (Small Baseline Subset) processing package developed and distributed by NRCan (Samsonov 2019) was then used to recover the deformation time-series for the period of InSAR observation (Figure 9).

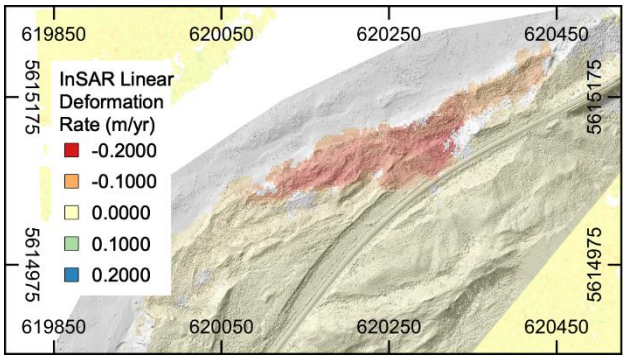

Figure 9. InSAR linear deformation rate map with semi-transparent hill-shade applied for context. Deformation rate is estimated from an InSAR time-series spanning January 5, 2021 to December 3rd 2021

4 RESULTS AND DISCUSSION

The following section summarizes a comparison of landslide deformation monitoring observations generated through RTK surveys, InSAR monitoring and RPAS surveys. Each of these methods has limitations that must be considered when comparing to other methods. Measurements vary in terms of directional sensitivity, frequency of observation, temporal coverage and absolute vs differential measurement. Two separate methods of comparison across these datasets are presented. The first method is to project the RTK measurements, 3D RPAS displacement to the RADAR satellite line-of-sight and compare the associated time-series profiles at all GCP positions. This method only considers a small subset of points available to both the wide-area RPAS and InSAR methods. However, it highlights agreements and differences throughout the time-series. The second comparison method leverages the broad spatial coverage of both the 3D RPAS measurements and InSAR by estimating the annual deformation rate of both datasets and comparing all collocated points.

Monitoring results generated from using the M3C2 point cloud comparison are not compared to monitoring results generated from other studies. This method calculates deformation along a vector normal to the ground surface and therefore the resulting estimated direction of deformation is highly variable. It would be technically possible to project these normal vectors into the InSAR line of sight vector or decompose the deformation vectors into their Cartesian components. However, this comparison would not be particularly meaningful. It is likely that M3C2 generally underestimates deformation in this type of landslide to a degree that varies with the alignment of the true deformation vector and the surface normal. M3C2 can be expected to output nearly accurate estimates of ground deformation on surfaces perpendicular to ground movement but is generally insensitive to surface-parallel movement.

4.1 RTK – InSAR – RPAS point comparison

A full InSAR time-series as well as the cumulative RPAS deformation measurements were extracted for points locations at each of the eleven GCPs where InSAR measurements were available. Differences in the RTK positions were calculated to construct a displacement time-series. Displacements in X, Y & Z were projected to the RCM line of sight for both the RTK and RPAS to create an accurate basis for comparison. Figures 10 to 12 show time-series profiles for three characteristic GCPs (i.e. NS-1, NS-7, NS-9, see Figure 8). The remaining GCP comparisons are available in the appendix.

In general, the RTK, RPAS and InSAR measurements agree to within several centimetres of cumulative deformation. At points with larger displacements, we note

that the InSAR measurements tend to be slightly lower than both the RTK and RPAS measurements. These plots highlight the dense temporal sampling of the InSAR when compared to the RTK and RPAS measurements which are collected manually in the field and less frequently.

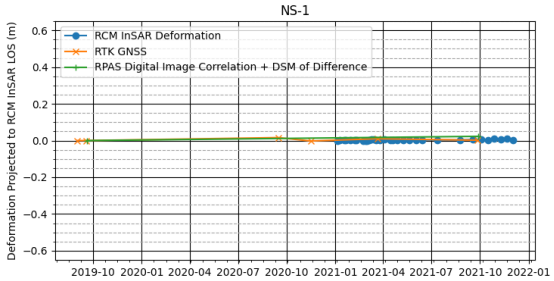

Figure 10. RCM, RTK, RPAS Deformation Time-Series Projected to RCM Line of Sight – NS-1

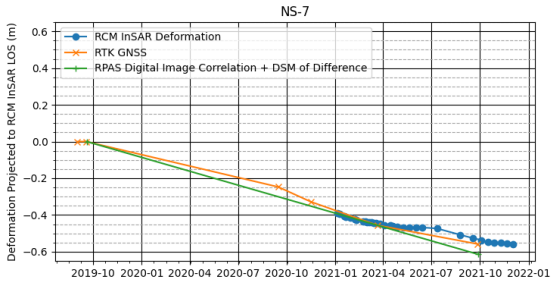

Figure 11. RCM, RTK, RPAS Deformation Time-Series Projected to RCM Line of Sight – NS-7

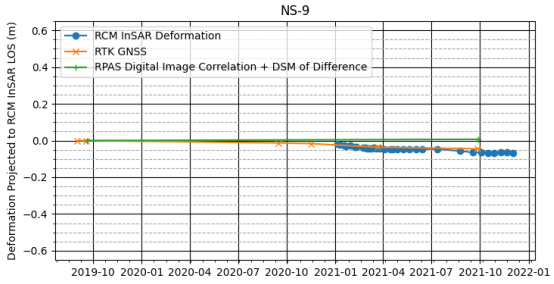

Figure 12. RCM, RTK, RPAS Deformation Time Series Projected to RCM Line of Sight – NS-9

4.2 InSAR - RPAS Wide Area Comparison

To examine a statistically significant number of points, the 3D RPAS deformation measurements were projected to the InSAR line of sight vector. This raster was then down-sampled and aligned to match the pixel geometry of the InSAR results. Overlapping pixels from the RPAS results and the InSAR results were considered resulting in 20,843 points of comparison. The RPAS deformation represented a 2-year cumulative measurement without intermediate points in the time-series while the InSAR data represented a temporally dense set of measurements over a nearly one year period.

For a scatter plot analysis, the RPAS cumulative deformation measurements were plotted against the InSAR annual rate map with the axes scaled 2:1 and a trend line scaled to match (Figure 13).

Due to conflicts with other RCM requests, the longest period between sequential InSAR pairs was 44 days. With the relatively small spatial footprint of this slide, unwrapped phase values beyond one phase cycle were not deemed reliable. This places an upper bound on the deformation rate where measurements are deemed robust. In this case, that bound was deemed to be 2.8 cm over 44 days or approximately 24 cm/year. This bound can be improved with a higher revisit frequency and is not as much of a limitation when the spatial extents of the movement zone are larger and vary gradually. Figure 13 distinguishes points in excess of this rate by colour.

Inspection of Figure 13 reveals a general agreement between the RPAS and InSAR deformation trends. The cluster of points around the origin represents most of the surveyed area where the surface is relatively stable and reveals a spread in RPAS points that is approximately an order of magnitude larger than the spread of the InSAR. For deforming points, a general agreement in rate is observed up to nearly 20 cm/year. However, at higher rates the InSAR deformation outputs tend to be lower in comparison to the RPAS deformation rates. This may be due to a combination of factors such as phase aliasing of rapid deformation or a tendency for SBAS to smooth transient high velocity deformation events. This may also be a result of an imperfect comparison as there is only partial temporal overlap (January 2021 to October 2021) between the two data sets and could be explained by a higher average rate in the period preceding the InSAR time-series, a lower average rate in the period following the final RPAS survey date or a combination of both. Points where significant volumes of material collapse or are eroded such as steep slopes near the river bank will also be under-reported by InSAR measurements.

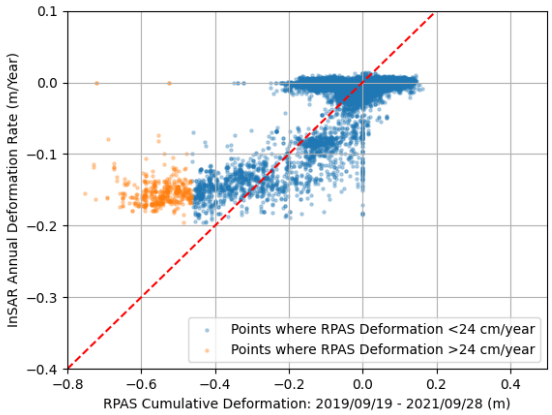

Figure 13. Wide area direct comparison of collocated InSAR and RPAS deformation. InSAR measurements represent a best fit annual rate while RPAS measurements represent 2 years of cumulative deformation. Note the 2:1 scaling to account for the difference in temporal periods.

A histogram was constructed by scaling the 2-year cumulative RPAS deformation by half to arrive at the closest estimate of an annual rate given the sampling frequency. These points were differenced with the InSAR annual rate at each coincident point to create a difference metric (Figure 14). Across 20,843 points, the 1σ and 2σ values were 0.025 m/year and 0.051 m/year, respectively. As in the scatter plot analysis, this is an imperfect comparison as the temporal overlap (January 2021 to October 2021) of the two datasets is not consistent.

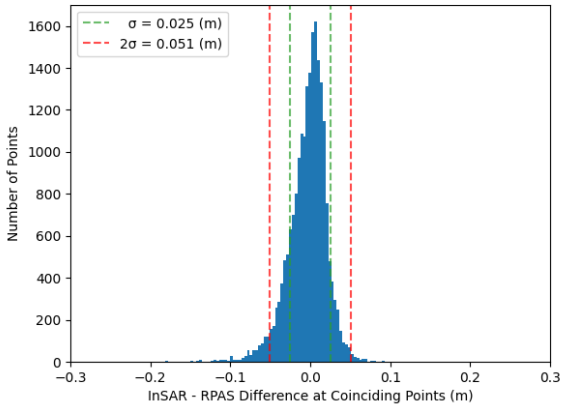

Figure 14. Histogram distribution of differences in collocated InSAR and RPAS deformation rates.

5 CONCLUSIONS

Each of the four methods in this study has strengths and limitations in the context of landslide monitoring. RTK surveying is well accepted as being both accurate and precise. However, collecting data is laborious and achieving wide area measurement coverage similar to what can be achieved with InSAR or RPAS surveying, even at small sites is impractical.

M3C2 is a fairly simple and accessible algorithm to run; it is free and open-source, and operates directly on point clouds which reduce the complexity of intermediate processing steps. The displacement magnitude of the M3C2 output may appear simple to interpret; however the variability in measurement direction and the insensitivity to surface parallel movement are major limitations for measuring landslides with rotational or translational movement. Because of the variation in movement direction, which is only measured on surface normals, change detection results generated using the M3C2 algorithm could not be directly compared with any other method discussed in this study.

The combination of RPAS digital image correlation and DSM of difference method was the only method that was able to provide a full three dimensional movement vector for each point with broad coverage across the landslide. Compared to M3C2, the processing requires more complexity and familiarity with a number of open-source tools. However, the outputs are more directly interpretable. Although the cumulative measurement did not reveal much insight into the landslide dynamics over time, the ability to visualize the 3D vector field across the landslide body revealed a level of insight into the spatial landslide dynamics which was not possible through any other method.

InSAR is the only method in this study that does not require a physical site visit. This value became particularly evident during a study period that included restrictions on non-essential travel in British Columbia (B.C). Our method allowed for a set of measurements that is not only broad in spatial coverage but also dense in temporal measurements which provided a level of insight into the seasonal dynamics of landslide movement, which was not possible, or at least practical, by any other method. The line-of-sight limitation of InSAR adds complexity to interpretation and satellite tasking. We found good agreement between our InSAR and 3D RPAS methodologies for stationary and lower deformation rates. However, in parts of the landslide where the deformation rate approached approximately 20 cm/year, we found that these InSAR measurements typically output lower rates than the 3D RPAS method. This may have been a result of an imperfect comparison of datasets with different measurement periods, an underestimation from InSAR of erosion and slope collapse or an issue with InSAR phase aliasing during periods of high deformation rates.

In general, the noise level for stationary and slowly deforming points was higher in the combined 3D RPAS methodology than in the InSAR. However, in areas of rapid deformation, the 3D RPAS did not appear to reflect the same underestimation apparent in the InSAR time-series measurements when compared to RTK.

Future improvements to these comparisons will be made through a wider temporal overlap in measurements and through longer time-series of collections. The RPAS deformation measurement techniques are currently limited only to a pair-wise analysis. However, a multi-temporal approach, similar to how SBAS is applied to InSAR would reveal not only spatial, but also temporal dynamics of the landslide body.

6 APPENDIX

Figure 15 to 22 show deformation time series measurements extracted from RCM InSAR, RTK and RPAS for all remaining North Slide GCP locations depicted in Figure 8 that were not included in section 4.1.

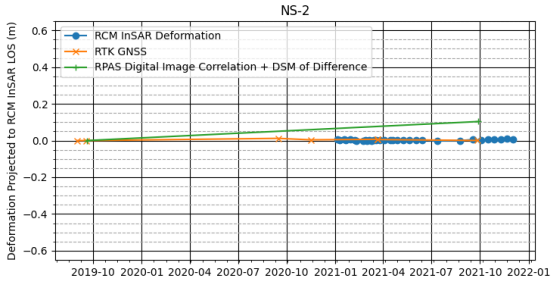

Figure 15. RCM, RTK, RPAS Deformation Time-Series Projected to RCM Line of Sight – NS-2

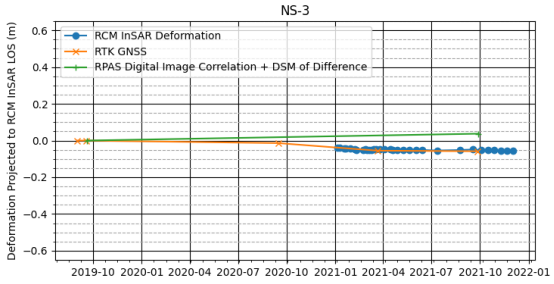

Figure 16. RCM, RTK, RPAS Deformation Time-Series Projected to RCM Line of Sight – NS-3

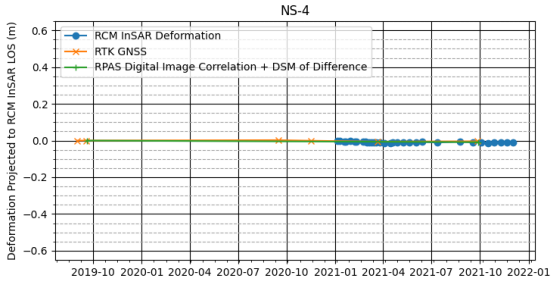

Figure 17. RCM, RTK, RPAS Deformation Time-Series Projected to RCM Line of Sight – NS-4

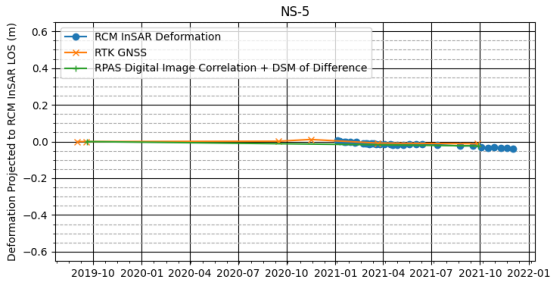

Figure 18. RCM, RTK, RPAS Deformation Time-Series Projected to RCM Line of Sight – NS-5

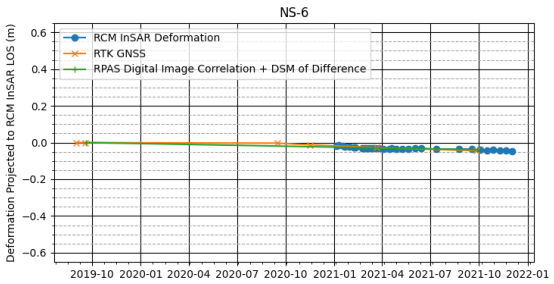

Figure 19. RCM, RTK, RPAS Deformation Time-Series Projected to RCM Line of Sight – NS-6

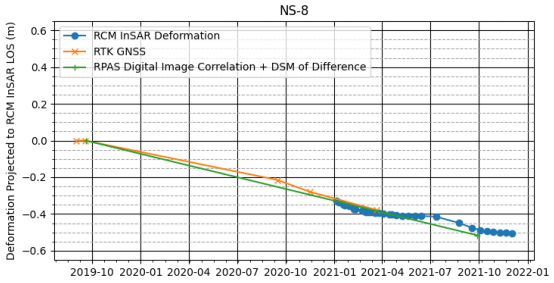

Figure 20. RCM, RTK, RPAS Deformation Time-Series Projected to RCM Line of Sight – NS-8

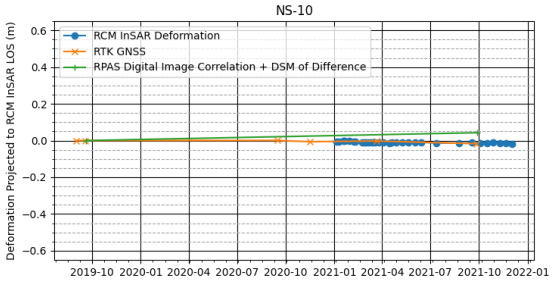

Figure 21. RCM, RTK, RPAS Deformation Time-Series Projected to RCM Line of Sight – NS-10

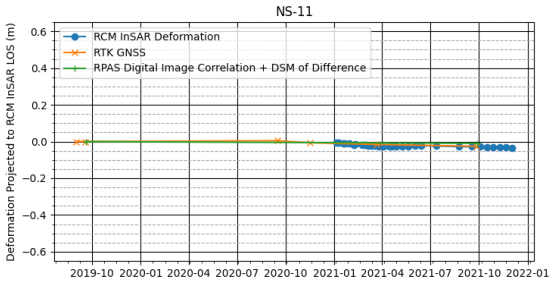

Figure 22. RCM, RTK, RPAS Deformation Time-Series Projected to RCM Line of Sight – NS-11

7 ACKNOWLEDGEMENTS

Field studies were made possible through the support of Danny Wong (Canadian Pacific Railways, Calgary, Alberta) and Trevor Evans (Canadian National Railways, Kamloops, BC).

8 FUNDING

This research was funded by Transport Canada and Natural Resources Canada.

9 REFERENCES

Clague, J., and Evans, S. 2003. Geologic framework for large historic landslides in Thompson River valley, British Columbia, *Environmental and Engineering Geoscience*, 9: 201–212.

Dudley, J.P. Samsonov, S.V. 2020. The Government of Canada automated processing system for change detection and ground deformation analysis from RADARSAT-2 and RADARSAT Constellation Mission Synthetic Aperture Radar data: description and user guide, *Geomatics Canada, Open File* 63: 65

Eshraghian, A., Martin, C. and Cruden, D. 2007. Complex earth slides in the Thompson River Valley, Ashcroft, British Columbia. *Environmental and Engineering Geoscience*, Vol. XIII: 161-181

Eshraghian, A., Martin, C. and Morgenstern, N. 2008. Movement triggers and mechanisms of two earth slides in the Thompson River Valley, British Columbia, Canada. *Canadian Geotechnical Journal*, 45: 1189-1209

Evans, S.G. 1984. The 1880 landslide dam on Thompson River, near Ashcroft, British Columbia. *Geological Survey of Canada, Current Research*, Part A, Paper 84-1A: 655–658, https://doi.org/10.4095/119628

Galland, O., Bertelsen, H. S., Guldstrand, F., Girod, L., Johannessen, R. F., Bjugger, F., Burchardt, S., and Mair, K. 2016. Application of open-source photogrammetric software MicMac for monitoring surface deformation in laboratory models, *Journal of Geophysical Research: Solid Earth,* 121: 2852– 2872,

Huntley, D., Bobrowsky, P., Charbonneau, F., Journault, J. and Hendry, M. 2017. Innovative landslide change detection monitoring: application of space-borne InSAR techniques in the Thompson River valley, British Columbia, Canada. *Landslide Research and Risk Reduction for Advancing Culture and Living with Natural Hazards*, Springer International Publishing: 13 p.

Huntley, D., Bobrowsky, P., MacLeod, R., Cocking, R., Joseph, J. and Rotheram-Clarke, D. 2021d. Ensuring resilient socio-economic infrastructure: field testing innovative differential GNSS-InSAR-UAV monitoring technologies in mountainous terrain near Ashcroft, British Columbia, Canada. *Journal of Mountain Science*, 18 (1): 1-20

Journault, J. Macciotta, R., Hendry, M., Charbonneau, F., Huntley, D. and Bobrowsky, P. 2018. Measuring displacements of the Thompson River valley landslides, south of Ashcroft, B.C., Canada, using satellite InSAR. *Landslides*,15: 621-636

Lague, D. Brodu, N. Leroux, J. 2013. Accurate 3D Comparison of Complex Topography with Terrestrial Laser Scanner: Application to the Rangitikei Canyon (N-Z). *ISPRS Journal of Photogrammetry and. Remote Sensing*, 82: 10–26.

Lucieer A, Jong SM de, Turner D. 2014. Mapping landslide displacements using Structure from Motion (SfM) and image correlation of multi-temporal UAV photography. *Progress in Physical Geography: Earth and Environment*, 38: 97-116.

Porter, M., Savigny, K., Keegan, T., Bunce, C. and MacKay, C. 2002. Controls on stability of the Thompson River landslides. Canadian Geotechnical Society, Ground and Water – Theory to Practice, *Proceedings of the 55th Canadian Geotechnical Conference*: pp.1393-1400

Rosu, A. Pierrot-Deseilligny, M. Delorme, A. Binet, R. Klinger, Y. 2015. Measurement of ground displacement from optical satellite image correlation using the free open-source software MicMac. *ISPRS Journal of Photogrammetry and Remote Sensing*, 100: 48-59

Rupnik, E., Daakir, M. & Pierrot Deseilligny, M. 2017. MicMac – a free, open-source solution for photogrammetry. *Open geospatial data, Software and Standards*, 2: 14

Samsonov, S V. 2019. User manual, source code, and test set for MSBASv3 (Multidimensional Small Baseline Subset version 3) for one- and two-dimensional deformation analysis. *Geomatics Canada, Open File*

Stanton, R.B. 1898. The great land-slides on the Canadian Pacific Railway in British Columbia. *Proceedings Civil Engineers*, 132(2): 1–48

Türk, T. 2018 Determination of mass movements in slow-motion landslides by the Cosi-Corr method. *Geomatics, Natural Hazards and Risk*, 9:1, 325-336